Bifurcation analysis of interacting stationary modes in thermohaline convection

M. Neveling and G. Dangelmayr
Institute for Information Sciences, University of Tübingen, Köstlinstrasse 6, D-7400 Tübingen, Federal Republic of Germany
(Received 14 March 1988)

The Boussinesq equations for thermohaline convection in a finite two-dimensional box and with stress-free boundaries are considered. There are critical values of the aspect ratio at which the conduction state becomes unstable to two different roll patterns simultaneously. Near such a critical value a center manifold reduction allows us to reduce the dynamical behavior of the Boussinesq equations to a standard normal form equation that describes the interaction of two stationary modes. We present explicit analytical expressions for the linear and nonlinear coefficients on which the normal form depends. A numerical investigation of these coefficients leads to a division of the space of parameters (Prandtl number, solute Rayleigh number, Lewis number) into various regions that give rise to qualitatively different bifurcation behavior. Besides those encountered in ordinary convection, a variety of further phenomena is found, in particular in a vicinity of double tricritical points.

I. INTRODUCTION

Double-diffusive convection problems are characterized by two different processes. Besides the heat diffusion which eventually drives the convection, a second gradient induces another diffusion process which may substantially alter the qualitative behavior of the convection states. In thermohaline convection a concentration gradient is established by salt reservoirs at the top and the bottom of the box containing the fluid. Depending on whether the salt migrates to the cold or warm boundary, this second gradient acts stabilizing or destabilizing on the conduction state. The salt diffusion can have a strong influence on the onset of convective motion. Whereas in the absence of salt the first instability, or primary bifurcation, always leads to steady convection states which bifurcate supercritical from the conduction state as the Rayleigh number increases, the thermohaline problem may exhibit overturning convection and subcritical or supercritical steady convection states, depending on the imposed concentration gradient (solute Rayleigh number) and on the ratio of the diffusivities (Lewis number).

A common tool for analyzing secondary or higher-order bifurcations in multiparameter problems is to investigate the solution in a neighborhood of a point in parameter space, where two or more primary bifurcations coalesce. If the primary bifurcations lead to steady states, then such a multiple-bifurcation point gives rise to the interaction of stationary modes. For two-dimensional Boussinesq convection in a finite box the interaction of two steady roll patterns with consecutive wave numbers has been analyzed by Knobloch and Guckenheimer.[1] These authors found two different kinds of behavior. For small Prandtl numbers a continuous transition between the two pure roll patterns takes place across a stable mixed-mode branch, i.e., a superposition of the roll patterns. Contrary to that, for large Prandtl numbers, the mixed-mode branch is unstable, and hysteretic behavior occurs involving both roll patterns. A similar kind of analysis was recently pursued for the first two modes in the case of an infinitely extended fluid layer with periodic boundary conditions imposed.[2,3] Here, besides mixed-mode branches, also traveling wave solutions were obtained.

The purpose of this paper is to investigate interactions of stationary modes for the problem of thermohaline convection. Apart from the scenarios occurring in the case of ordinary convection, we find a variety of further phenomena, for example, subcritical pure-mode branches connected by a mixed-mode branch, and unbounded-mixed mode branches. We classify the different scenarios according to the theory of imperfect bifurcations[4] and present a detailed discussion of the regions in the space of the parameters (Prandtl number, solute Rayleigh number, and Lewis number) where these scenarios occur. In Sec. II we derive the normal form for mode interactions and present expressions for the relevant linear and cubic coefficients on which the normal form depends. In Sec. III we describe results of a numerical investigation of these coefficients which leads to a division of the parameter space into regions giving rise to qualitatively different bifurcation behavior. In Sec. IV our results are compared with those of Ref. 1 and an outlook is given on further open questions and problems. Mathematical details are summarized in two Appendixes.

II. DERIVATION OF THE NORMAL FORM

Thermohaline Boussinesq convection in a two-dimensional box is described by the equations

$$\frac{1}{\sigma}\left[\frac{\partial}{\partial t}\nabla^2\psi + J(\psi,\nabla^2\psi)\right] = \nabla^4\psi + R\,\Theta_x - R_S\,\Gamma_x \ , \tag{1a}$$

$$\frac{\partial\Theta}{\partial t} + J(\psi,\Theta) = \psi_x + \nabla^2\Theta \ , \tag{1b}$$

$$\frac{\partial\Gamma}{\partial t} + J(\psi,\Gamma) = \psi_x + \tau\nabla^2\Gamma \ , \tag{1c}$$

$$\psi=\psi_{zz}=\Theta=\Gamma=0 \quad \text{for } z=0,1 \ , \tag{1d}$$

$$\psi=\psi_{xx}=\Theta_x=\Gamma_x=0 \quad \text{for } x=0,l \ , \tag{1e}$$

where $J(f,g)=f_x g_z-f_z g_x$. Here, ψ is the nondimensionalized stream function, Θ and Γ describe deviations of the temperature and concentration fields from the basic conduction state, and R, σ, R_S, and τ are, respectively, the (thermal) Rayleigh number, the Prandtl number, the solute Rayleigh number, and the Lewis number.[5] The system of partial differential equations (1a)–(1c) is valid inside the box $\{(x,z):0\le x\le l,\ 0\le z\le 1\}$, with the boundary conditions (1d) and (1e) corresponding to temperature and concentration fixed at the top and bottom, no sideways heat and concentration fluxes, and no tangential viscous stresses. The concentration gradient of the conduction state is proportional to the solute Rayleigh number and is induced by reservoirs at the top and the bottom. This is in contrast to convection in binary fluids, where the concentration gradient originates from the Soret effect which has been neglected in (1c).

For all values of R, σ, R_S, and τ Eqs. (1) admit the basic conduction solution $\psi=\Theta=\Gamma=0$. Setting $U=(\psi,\Theta,\Gamma)^T$, the linearized equations (1) possess a nontrivial stationary solution of the form

$$U=U_k(x,z) \equiv \begin{pmatrix} (k^2+l^2)\pi^2\sin(k\pi x/l) \\ kl\pi\cos(k\pi x/l) \\ (kl\pi/\tau)\cos(k\pi x/l) \end{pmatrix} \sin(\pi z) \ , \tag{2}$$

when $R=R_c^k(l)$, i.e., the conduction state encounters a stationary bifurcation. Here, $k=1,2,\ldots$, and

$$R_c^k(l)\equiv R_S/\tau+R_0(k,l) \ , \tag{3a}$$

where

$$R_0(k,l)\equiv\frac{\pi^4(k^2+l^2)^3}{k^2l^4} \tag{3b}$$

is the critical Rayleigh number for the ordinary Bénard problem without an imposed concentration gradient ($R_S=0$). For fixed k we require that the first instability occurs at $R=R_c^k(l)$ when R is increased from below. This leads to the following two conditions. (i) The aspect ratio l is restricted to the range $l_{k-1}<l<l_k$, with the critical aspect ratios l_j ($j=1,2,\ldots$) given by

$$l_j=[j(1+j)]^{1/3}[j^{2/3}+(j+1)^{2/3}]^{1/2} \ . \tag{4}$$

This condition guarantees that $R_c^k(l)$ is the minimum value in the set $\{R_c^j(l),\ j=1,2,\ldots\}$. (ii) We have to exclude overturning convection to occur before the stationary instability. This restricts R_S to[6]

$$R_S<R_{S,c}\equiv R_0\frac{\tau^2(1+\sigma)}{\sigma(1-\tau)} \quad \text{if } \tau<1 \ , \tag{5}$$

whereas for $\tau>1$ no oscillatory instability exists if $R>0$. We assume that the fluid is always heated at the bottom, i.e., that the Rayleigh number R is positive. Consequently $R_c^k(l)>0$ which leads to a further restriction on R_S, viz.,

$$R_S>R_{S,\min}\equiv-\tau R_0(k,l) \ . \tag{6}$$

When (5) and (6) are satisfied and $l_{k-1}<l<l_k$, then the conduction state is stable for $0<R<R_c^k(l)$, but loses stability to exponentially growing solutions of the form $e^{st}U_k(x,z)$ [$\mathrm{Re}(s)>0$] for $R>R_c^k(l)$.

When the width is adjusted such that $l=l_k$ we find $R_c^k(l_k)=R_c^{k+1}(l_k)\equiv R_k$. This means that two modes with horizontal wave numbers k and $k+1$ become unstable simultaneously giving rise to a bifurcation of codimension 2. In this paper we are interested in analyzing the behavior of (1a)–(1c) for parameters values (R,l) close to (R_k,l_k). In the ordinary Bénard problem this simultaneous instability occurs for $(R,l)=(R_{0k},l_k)$ [$R_{0k}\equiv R_0(k,l_k)$] and has been analyzed in Ref. 1.

In the vicinity of (R_k,l_k) the dynamics of (1a)–(1c) will contract to a two-dimensional center manifold. The center manifold can be parametrized by coordinates of the neutrally stable eigenspace of the linearized equations, i.e., by the amplitudes of the unstable modes U_k and U_{k+1} which are denoted by X and Y, respectively. The center manifold reduction then yields a system of ordinary differential equations for (X,Y) which, owing to the $Z(2)\times Z(2)$ symmetry of (1a)–(1c), has the form

$$\dot X=-(AX^3+BXY^2-\alpha X)+\cdots \ , \tag{7a}$$

$$\dot Y=-(CX^2Y+DY^3-\beta Y)+\cdots \ , \tag{7b}$$

where the dots represent terms of higher order. The linear coefficients α,β are unfolding parameters depending on $R-R_k$ and $l-l_k$. To linear order they are given by

$$\begin{pmatrix}\alpha\\ \beta\end{pmatrix}=\begin{pmatrix} p_k & q_k \\ p_{k+1} & q_{k+1}\end{pmatrix}\begin{pmatrix} R-R_k \\ l-l_k\end{pmatrix} \ , \tag{8}$$

where

$$p_j=\sigma j^2 l_k^2/(\pi^2 a_j^4), \quad q_j=(2\sigma\pi^2/l_k^3)(2j^2-l_k^2) \tag{9a}$$

with

$$a_j^2=j^2+l_k^2 \quad (j=k,k+1) \ . \tag{9b}$$

The calculation of the nonlinear coefficients A,B,C,D is very tedious and has been performed by means of a 14-mode representation for the solutions of (1). The main steps of the calculation are summarized in Appendix A, here we present the results. The pure-mode coefficients A,D are given by

$$A=(\sigma k^2\pi^2/8l_k^2)[1+(R_S/R_{0k})(\tau^2-1)/\tau^3] \ , \tag{10a}$$

$$D=[\sigma(k+1)^2\pi^2/8l_k^2][1+(R_S/R_{0k})(\tau^2-1)/\tau^3] \ . \tag{10b}$$

The mixed coefficient B has the form

$$\begin{aligned} B=&B_{-1}/\sigma+B_0[1+(R_S/R_{0k})(\tau-1)/\tau^2] \\ &+\sigma[B_{11}+(R_S/R_{0k})(B_{12}/\tau^3+B_{13}/\tau^2+B_{14}/\tau) \\ &+B_{15}(R_S/R_{0k})^2(1-2\tau-\tau^2)/\tau^4] \ . \end{aligned} \tag{11}$$

An analogous formula holds for C, with B_{-1},B_0,B_{1j} ($j=1,2,3,4,5$) replaced by C_{-1},C_0,C_{1j}. These expressions depend only on k and are presented in Appendix B.

III. ANALYSIS OF THE NORMAL FORM

In Sec. II we have reduced the Boussinesq equations (1a)–(1c) to the normal form (7) which is valid in a neighborhood of $(R,l)=(R_k,l_k)$. This normal form has been discussed by several authors in different contexts (see, e.g., Refs. 4 and 7) and is well understood. A study of its dynamics involves locating fixed points, analyzing their stability, and using the divergence test to locate possible limit cycles. The behavior of (7) depends crucially on the signs of A,D and of the determinant $d_0\equiv AD-BC$ so that a number of cases has to be distinguished. There are three types of steady states: the trivial solution T ($X=Y=0$), single-mode solutions S_X and S_Y with ($X\neq 0, Y=0$) and ($X=0, Y\neq 0$), respectively, and mixed-mode solution S_{XY}, where both X and Y are nonzero. If $AD>0$ oscillations do not occur, if $AD<0$, a limit cycle is created through a Hopf bifurcation from the mixed-mode branch. From (10) we infer that A and D cannot have opposite signs, i.e., the Hopf bifurcations do not occur. This means that the expansion to cubic order in (7) is sufficient. (The stability of bifurcating limit cycles is determined by fifth-order terms; however, the type of the steady states is completely fixed by the cubic terms.)

In Fig. 1 we have sketched the stability diagrams in the (α,β) plane for the six qualitatively distinct cases of (7) that occur if $AD>0$. The dynamical behavior is completely determined by the steady states, thus we have confined ourselves to the existence and the type of the steady states in dependence of the "unfolding parameters" α and β. For each case of Fig. 1 the (α,β) plane is divided into six regions by the axes (primary bifurcations) and the lines L_X,L_Y (secondary bifurcations). In each region we find a certain configuration of steady states with specific stabilities. The existence of a nontrivial steady state (S_X, S_Y, or S_{XY}) is indicated by a curved line passing through the regions in which it exists. Stabilities are characterized by the stability assignments, i.e., by the signs of the real parts of the eigenvalues corresponding to the linearized matrix. Solutions with assignment $(--)$ are stable, all other solutions are unstable. For S_X and S_Y the stability assignments change when the lines L_X and L_Y are crossed, respectively. The trivial steady state exists for all values of (α,β) with assignments $(++)$ in $\{\alpha>0,\beta>0\}$, $(--)$ in $\{\alpha<0,\beta<0\}$, and $(+-)$ in $\{\alpha\beta<0\}$.

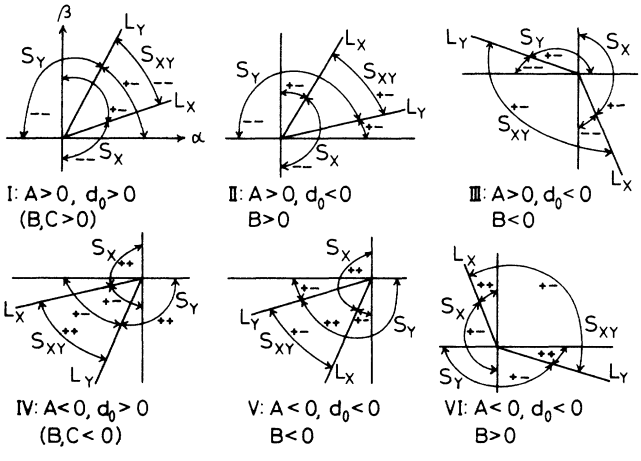

FIG. 1. Stability diagrams for normal form (7) with $AD>0$. Here, $d_0=AD-BC$ and L_X:$\beta=(C/A)\alpha$ ($A\alpha>0$), L_Y:$\alpha=(B/D)\beta$ ($D\beta>0$). To case I there correspond actually four different subcases depending on the signs of B,C. Changing $B>0$ to $B<0$ moves L_X across the α axis and analogously for C. A similar situation holds for case IV.

Convection experiments are usually performed in a particular box where the Rayleigh number is varied by successively increasing the temperature at the bottom. Therefore we are interested in bifurcation diagrams which exhibit for fixed l the behavior of the steady states of (7) in dependence of $R-R_k$. Generic bifurcation diagrams associated with (7) are discussed in detail in Ref. 4, here we shortly review these results in terms of the physical parameters. When l is fixed near l_k and $R-R_k$ is varied from below, the (α,β) plane is traversed by a (approximately straight) path passing through the various regions of a stability diagram of Fig. 1. The path corresponding to $l=l_k$ passes through the origin and will be called the basic path. For $l\neq l_k$ the basic path is distorted to a generic path giving rise to a generic bifurcation diagram. The qualitative type of these diagrams depends crucially on the position of the basic path relative to the secondary bifurcation lines L_X,L_Y. Since $p_k,p_{k+1}>0$ each basic path passes from the region $\{\alpha<0,\beta<0\}$ ($R<R_k$) to $\{\alpha>0,\beta>0\}$ ($R>R_k$). For the stability diagrams I, II, IV, and V the basic path can be located below, above, or inside the region in which the S_{XY} solution exists, i.e., there are three cases to be distinguished. Which of these cases occurs depends on the determinants

$$d_1=Ap_{k+1}-Cp_k,\quad d_2=Bp_{k+1}-Dp_k\ . \tag{12}$$

If $d_1=0$ and $d_2=0$ the basic path is tangent to L_X and L_Y, respectively. The different cases for a basic path correspond to different sign combinations of d_1,d_2. Numerical investigations of these determinants show that for the stability diagrams I, II, and V two different cases Ia, IIa, Va and Ib, IIb, Vb occur, whereas for III and IV the determinants d_1,d_2 do not change sign. Specifically we find

$$\begin{aligned} &d_1<0,\quad d_2<0 \quad \text{for Ia, IIa, IV, Va}\ ,\\ &d_1<0,\quad d_2>0 \quad \text{for IIb}\ ,\\ &d_1>0,\quad d_2<0 \quad \text{for Ib, III, Vb}\ . \end{aligned} \tag{13}$$

The stability diagram VI does not appear in the thermohaline problem. Because $q_k<0<q_{k+1}$, a generic path with $l<l_k$ intersects first the β axis and then the α axis, and conversely for $l>l_k$, i.e., to each case there correspond two different generic bifurcation diagrams. The

basic and the distorted paths for Ia and Ib are shown in Fig. 2. In Fig. 3 we have sketched the generic bifurcation diagrams corresponding to the cases summarized in (13). Observe that the S_{XY} branches are unbounded for Ib, IIb, Vb and bounded for the other cases.

The task is now to locate the different cases of (13) in the space of the physical parameters. Since the Rayleigh number and the length are fixed by $R=R_k$ and $l=l_k$, we have to investigate the (σ,R_S,τ) space. This space must be divided into different regions such that each region corresponds to one of the cases of (13), distinguished by the signs of A,D,B or C,d_0,d_1,d_2. We represent the division of the (σ,R_S,τ) space in the (R_s,τ) plane for fixed Prandtl number σ. The coefficients A,D vanish along the line of "tricritical points"

$$\text{TC:}\quad R_{S,\text{tri}}(\tau)=R_0\tau^3/(1-\tau^2)\ , \tag{14}$$

which only for $\tau<1$ is inside the physically allowed region, defined by [cf. (5) and (6)]

$$R_{S,\min}(\tau)<R_S<R_{S,c}(\tau)\ . \tag{15}$$

The line TC constitutes one of the boundaries in the (R_S,τ) plane separating the various regions. The other boundaries are given by

$$d_0=0,\quad d_1=0,\quad d_2=0\ . \tag{16}$$

We have analyzed these equations numerically for $1\le k\le 10$. For all of these values we found the same qualitative behavior. There are three critical values $\sigma_1<\sigma_2<\sigma_3$, tabulated in Table I, such that the division of the (R_S,τ) plane undergoes a qualitative change when σ crosses one of these values. The results of our numerical computations are sketched schematically in Figs. 4(a)–4(d). We find two branches of $d_0=0$, distinguished by large (upper branch) and small (lower branch) values of R_S (solid line in Fig. 4). The equation $d_1=0$ possesses a branch with $R_s>0$ and for $d_2=0$ we find a branch with $R_S<0$ (dashed-dotted lines). For $0<\sigma<\sigma_1$ the upper $\{d_0=0\}$ branch lies to the left of TC [Fig. 4(a)]. When σ increases this branch becomes tangent to TC for $\sigma=\sigma_1$ and develops two intersections for $\sigma>\sigma_1$ [Figs. 4(b) and 4(c)]. A similar event takes place for $\{d_1=0\}$ so that the lines $\{d_0=0\}$, $\{d_1=0\}$, and TC have two common intersections giving rise to the appearance of region III and Ib. These threefold intersections occur because TC is actually a line of double tricritical points where both coefficients A and D vanish. (If $A=D=d_0=0$ it follows that $d_1=0$ or $d_2=0$). For $0<\sigma<\sigma_2$ the lower $\{d_0=0\}$ branch terminates on the boundary line $M:R_S=R_{S,\min}(\tau)$ of the physically allowed region. This termination point moves towards infinity when σ approaches σ_2 and disappears for $\sigma>\sigma_2$. A similar event happens for $\{d_2=0\}$. When $\sigma_2<\sigma<\sigma_3$ the lower $\{d_0=0\}$ branch is still located below the τ axis [Fig. 4(c)], it coincides with the τ axis for $\sigma=\sigma_3$ and moves into the region $\{R_S>0\}$ for $\sigma>\sigma_3$ [Fig. 4(d)].

To give an impression of the scales hidden in Fig. 4 we note that the lower of the two triple intersections occurring in Figs. 4(b) and 4(c) is typically in a range between $R_S\approx 1500$ and $R_S\approx 10^4$, whereas the upper one lies between $R_S\approx 10^4$ and $R_S\approx 2\times 10^4$. On the other hand, on

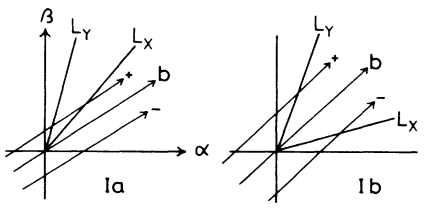

FIG. 2. Paths in the (α,β) plane traced out by varying $R-R_k$ from below for fixed l. b: basic path for $l=l_k$. Perturbed paths for $l>l_k$ and $l<l_k$ are marked by $+$ and $-$. Cases Ia and Ib are distinguished by $d_1<0$, $d_2<0$ and $d_1>0$, $d_2<0$, respectively.

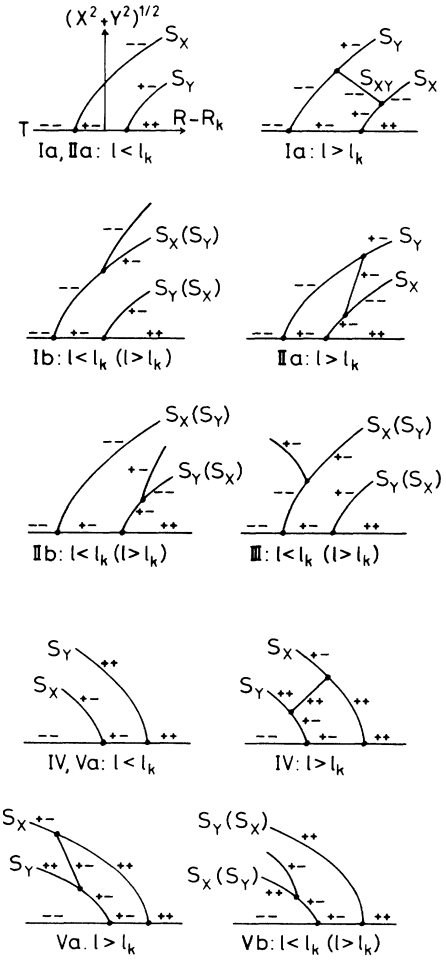

FIG. 3. Bifurcation diagrams for fixed $l\neq l_k$ corresponding to paths through the stability diagrams I–V of Fig. 1. T: trivial solution $X=Y=0$ (conduction state). S_X,S_Y: branches of single-mode solutions. S_{XY}: branch of mixed-mode solutions bifurcating from a single-mode branch.

TABLE I. Critical Prandtl numbers $\sigma_1, \sigma_2, \sigma_3$.

	$k=1$	$k=2$	$k=3$	$k=4$	$k=5$	$k=6$	$k=7$	$k=8$	$k=9$	$k=10$
σ_1	0.117	0.092	0.067	0.052	0.043	0.037	0.033	0.029	0.026	0.023
σ_2	0.377	0.239	0.188	0.161	0.144	0.131	0.121	0.113	0.107	0.101
σ_3	0.402	0.251	0.200	0.172	0.154	0.141	0.130	0.122	0.155	0.110

the lower $\{d_0=0\}$ branch R_S varies for $\tau=1$ between $R_S\approx -100$ and $R_S\approx 20$. It is, therefore, impossible to present a quantitatively correct version of Fig. 4 without using different scales for different regions. Thus we have confined ourselves to a qualitative picture.

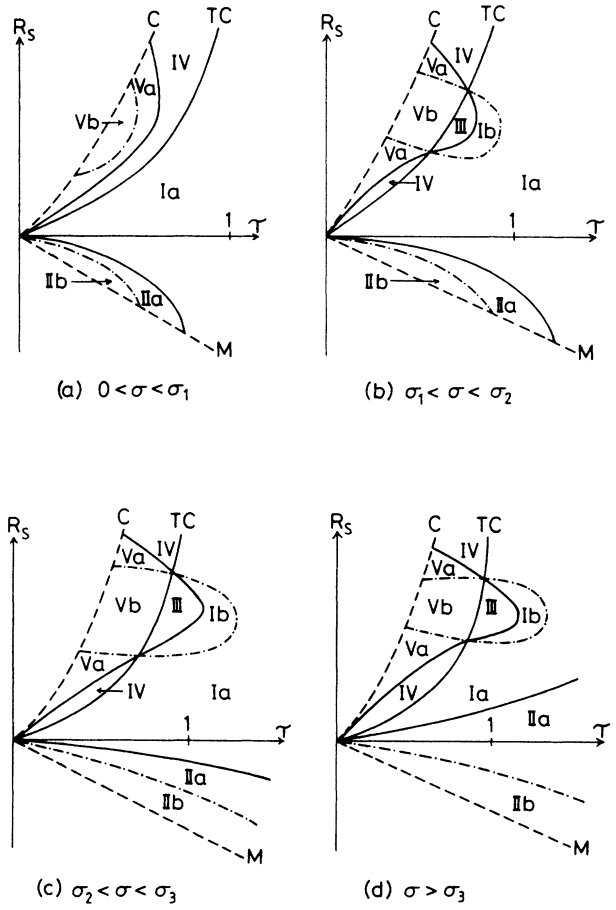

FIG. 4. Schematic representation of the (R_S,τ) plane for different generic values of σ. TC denotes the line of tricritical points [$A=D=0$, Eq. (14)], all other solid lines are branches of $\{d_0=0\}$. The dashed lines C: $R_S=R_{S,c}$ and M: $R_S=R_{S,\min}$ constitute the boundaries of the physically allowed region. C and TC approach $\{\tau=1\}$ asymptotically for $R_S\to\infty$. The solid lines separate the regions corresponding to the different stability diagrams of Fig. 1 (Roman numerals). Regions I, II, and IV are further divided into subregions Ia, Ib, etc. by the dashed-dotted lines giving rise to the different bifurcation diagrams of Fig. 3. On the dashed-dotted lines above and below the τ axis we have $d_1=0$ and $d_2=0$, respectively. No attempts are made to preserve scales.

IV. DISCUSSION

We have studied thermohaline Boussinesq convection in a finite two-dimensional box near a double critical point, where two consecutive modes become unstable simultaneously. This extends the work of Guckenheimer and Knobloch,[1] who analyzed this multiple instability for ordinary convection problems. Our problem reduces to that considered in Ref. 1 if τ is large and $|R_S|$ is sufficiently small. In that case we recover essentially the results of Ref. 1. For small σ the stability diagram I occurs, whereas for larger Prandtl number the determinant d_0 has changed its sign, leading to the stability diagram II. A glance at Fig. 4 shows that this behavior holds actually for all $\tau>0$, provided R_S, i.e., the imposed concentration gradient, is sufficiently small. It is obvious that our σ_3 should coincide with the critical Prandtl number σ_c of Ref. 1. A comparison of the numerical results shows that this is indeed the case for $k=3$ and $k=4$, however, there is a disagreement for $k=1$ and $k=2$. The values $\sigma_c(k=1)=0.30$ and $\sigma_c(k=2)=0.22$ of Ref. 1 are smaller than our results for σ_3 (cf. Table I). The reason for this disagreement is not yet clear. Knobloch and Guckenheimer have also found that the coefficient B is negative for very small σ and changes sign at some $\sigma<\sigma_c$. This result agrees with our calculations, but we have not included a discussion of the zeros of B,C in Fig. 4 because we concentrated on the bifurcation diagrams which are determined by d_1,d_2. We note that in the limiting case of ordinary convection the S_{XY} branches of the bifurcation diagrams are always bounded, giving rise to a continuous transition from a stable $(k+1)$ mode to a stable k mode across a stable mixed-mode branch (case Ia of Fig. 3), or to hysteretic behavior of the pure modes in virtue of an unstable S_{XY} branch (case IIa). This also agrees with the results of Ref. 1.

When R_S is negative the diffusions of salt and heat are both destabilizing effects for the conduction state. This means that we should expect similar behavior as an ordinary convection, but with the stationary instability occurring at a smaller Rayleigh number. For small $|R_S|$ this is indeed the case, however, if we come close to the line $M:R_S=R_{S,\min}(\tau)$, we find bifurcation diagrams of the type IIb, i.e., unbounded mixed-mode branches and globally stable coexisting single-mode solutions. At this point we mention that our analysis is strictly local and that more global information can be inferred by analyzing higher degeneracies. Presumably an analysis near the lower broken dotted line of Fig. 4 reveals that the S_{XY} branch in the diagram IIb for $l<l_k$ (Fig. 3) returns back to the S_Y branch, thereby producing again an unstable S_Y, whereas for $l>l_k$ the S_{XY} branch connects S_X and

S_Y as in the case IIa. Similar scenarios are expected in the regions Ib, III, and Vb of Fig. 4.

More complex phenomena appear if the salt diffusion is stabilizing and heat diffuses faster than salt, i.e., if $R_S > 0$ and $\tau < 1$. To the left of the line C in Fig. 4 overturning convection advances the stationary instabilities[6] which was not the subject of our investigations. Between C and TC both primary bifurcations are subcritical, leading to unstable single-mode and mixed-mode solutions (diagrams IV, Va, and Vb of Fig. 3). To the right of the tricritical line TC we find for very small σ only the diagrams Ia, but for $\sigma > \sigma_1$ also the diagrams Ib and III occur, both having unbounded S_{XY} branches. It is important to note that both cubic coefficients A and D vanish simultaneously along TC so that this line is actually a line of a double tricritical point. This fact excludes simultaneous super- and subcritical bifurcations of the two single-mode branches and, therefore, tertiary Hopf bifurcations[4] from S_{XY}. The impossibility of Hopf bifurcations was already demonstrated in Ref. 8 and has recently also been mentioned in Ref. 9. We regard the simultaneous vanishing of both cubic coefficients A and D as ungeneric and consider it as an artifact of the Boussinesq approximation. Generically the line TC should be split into two lines and between these lines Hopf bifurcations from S_{XY} can be expected. We hope to be able to achieve this splitting by including non-Boussinesq terms, but this deserves further study.

Of special interest in Figs. 4(b)–4(d) are the two triple intersections where the three cubic coefficients A, D, and C vanish simultaneously. Near these points the system (7) has to be expanded to at least fifth order. Quintic pure-mode coefficients (corresponding to X^5, Y^5) have already been computed,[10] but mixed-mode coefficients of this order (e.g., for X^2Y^3) did not yet appear in the literature. When σ approaches σ_1, the two triple intersections merge which constitute the highest degeneracy following from our study. A bifurcation analysis near this point should provide a lot of information about the dynamical behavior of (1) in the regions Ia, Ib, IV, Va, and Vb of Fig. 4. Specifically we expect that such an analysis will show that the single-mode branches of the diagrams IV, Va, and Vb of Fig. 3 bend back to the forward direction by means of a saddle-node bifurcation as in the single tricritical case[10] and that also oscillatory behavior can be present.

ACKNOWLEDGMENT

Helpful discussions with W. Güttinger and E. Knobloch are gratefully acknowledged.

APPENDIX A

The first step in the derivation of (7) is to expand the fields ψ, Θ, Γ into a finite number of modes which are relevant for the linear and cubic terms. Setting $\xi = \pi x / l_k$ and $f^1 = \Theta$, $f^2 = \Gamma$, the modes that contribute to this order are given by

TABLE II. Numerical values of the coefficients B_{-1}, C_{-1}, B_0, etc. and of l_k and R_{0k}.

	$k=1$	$k=2$	$k=3$	$k=4$	$k=5$	$k=6$	$k=7$	$k=8$	$k=9$	$k=10$
B_{-1}	−1.180 788	−0.070 845	−0.043 952	−0.032 094	−0.025 387	−0.021 051	−0.018 005	−0.015 743	−0.013 993	−0.012 598
B_0	−0.124 759	−0.039 142	−0.022 586	−0.016 098	−0.012 640	−0.010 469	−0.008 967	−0.007 858	−0.007 003	−0.006 321
B_{11}	1.534 036	1.407 976	1.355 378	1.326 989	1.309 273	1.297 194	1.288 434	1.281 793	1.276 586	1.272 395
B_{12}	−1.464 510	−1.366 300	−1.326 575	−1.305 131	−1.291 721	−1.282 546	−1.275 874	−1.270 805	−1.266 823	−1.263 612
B_{13}	−0.139 051	−0.083 352	−0.057 605	−0.043 697	−0.035 103	−0.029 296	−0.025 119	−0.021 976	−0.019 527	−0.017 565
B_{14}	0.188 320	0.116 485	0.082 673	0.063 861	0.051 967	0.043 786	0.037 822	0.033 283	0.029 714	0.026 835
B_{15}	0.069 525	0.041 676	0.028 802	0.021 848	0.017 551	0.014 648	0.012 559	0.010 988	0.009 763	0.008 782
C_{-1}	0.227 358	0.082 144	0.049 029	0.032 094	0.027 264	0.022 368	0.018 981	0.016 495	0.014 591	0.013 085
C_0	0.213 250	0.062 820	0.033 584	0.022 466	0.016 797	0.013 399	0.011 143	0.009 539	0.008 340	0.007 411
C_{11}	1.655 344	1.439 478	1.371 216	1.337 285	1.316 885	1.303 238	1.293 455	1.286 094	1.280 353	1.275 748
C_{12}	−1.679 259	−1.468 271	−1.393 938	−1.355 590	−1.332 115	−1.316 246	−1.304 795	−1.296 140	−1.289 366	−1.283 919
C_{13}	0.047 829	0.057 586	0.045 444	0.036 609	0.030 459	0.026 017	0.022 680	0.020 090	0.018 025	0.016 342
C_{14}	−0.213 309	−0.126 424	−0.087 738	−0.066 904	−0.053 990	−0.045 227	−0.038 899	−0.034 118	−0.030 381	−0.027 380
C_{15}	−0.023 914	−0.028 793	−0.022 722	−0.018 304	−0.015 229	−0.013 008	−0.011 340	−0.010 045	−0.009 012	−0.008 171
l_k	2.026 63	3.479 91	4.910 24	6.333 3	7.753 1	9.171 2	10.588	12.004 6	13.420 5	14.836 1
R_0	769.233	694.281	675.836	668.491	664.826	662.734	661.427	660.557	659.947	659.504

$$\psi(t,x,z)=\{A_k(t)\sin(k\xi)+A_{k+1}(t)\sin[(k+1)\xi]\sin(\pi z)+\{A_1(t)\sin(\xi)+A_{2k+1}(t)\sin[(2k+1)\xi]\}\sin(2\pi z)\ ,$$
$$f^j(t,x,z)=\{B_k^{(j)}(t)\cos(k\xi)+B_{k+1}^{(j)}(t)\cos[(k+1)\xi]\sin(\pi z)+\{C^{(j)}(t)+B_1^{(j)}(t)\cos(\xi)+B_{2k+1}^{(j)}(t)\cos[(2k+1)\xi]\sin(2\pi z)\ , \tag{A1}$$

where $j=1,2$. Substituting the expressions (A1) into Eqs. (1), representing products of trigonometric functions by sums, and neglecting modes which are not contained in (A1), we obtain the following system of 14 ordinary differential equations for the modal amplitudes A_k, A_{k+1}, $B_k^{(j)}$, . . . (dots denote time derivatives):

$$(l/\pi)^2(n^2+l^2)\dot{A}_n+\sigma(n^2+l^2)^2A_n+\sigma n(l/\pi)^3(R_sB_n^{(2)}-RB_n^{(1)})+A_1A_m\mu_n(2k+1)(1-m^2+3l^2)l/4$$
$$-A_{2k+1}A_m\mu_n[(2k+1)^2-m^2+3l^2]l/4=0\ , \tag{A2a}$$

$$(l/\pi)^2(r^2+4l^2)\dot{A}_r+\sigma(r^2+4l^2)^2A_r+\sigma(l/\pi)^3(R_sB_r^{(2)}-RB_r^{(1)})+A_kA_{k+1}\mu_r\epsilon_r(2k+1)l/4=0\ , \tag{A2b}$$

$$(l/\pi)^2\dot{B}_n^{(j)}+\tau_j(n^2+l^2)B_n^{(j)}-(l/\pi)nA_n-nlA_nC^{(j)}-(2k+1)(A_mB_1^{(j)}+\mu_nA_1B_m^{(j)})l/4$$
$$-\mu_n(A_{2k+1}B_m^{(j)}+A_mB_{2k+1}^{(j)})l/4=0\ , \tag{A2c}$$

$$(l/\pi)^2\dot{B}_r^{(j)}+\tau_j(r^2+4l^2)B_r^{(j)}-(l/\pi)rA_r+\epsilon_r(A_{k+1}B_k^{(j)}+\mu_rA_kB_{k+1}^{(j)})l/4=0\ , \tag{A2d}$$

$$(l/\pi)^2\dot{C}^{(j)}+4\tau_jl^2C^{(j)}+A_kB_k^{(j)}kl/2+A_{k+1}B_{k+1}^{(j)}(k+1)l/2=0\ , \tag{A2e}$$

where

$$\tau_1=1,\ \tau_2=\tau,\ \rho_1=k,\ \rho_{2k+1}=-1\ ,\ \epsilon_k=\epsilon_{2k+1}=1,\ \epsilon_{k+1}=\epsilon_1=2k+1\ ,$$
$$\mu_1=\mu_k=1,\ \mu_{k+1}=\mu_{2k+1}=-1\ . \tag{A3}$$

Here, $(n,m)=(k,k+1),(k+1,k)$ in (A2a) and (A2c), $r=1,2k+1$ in (A2b) and (A2d), and $j=1,2$ in (A2c)–(A2e). By construction, when $l=l_k$, $R=R_k$, the linearized problem of (A2) has two zero eigenvalues, the remainder having negative real parts. It follows that in a vicinity of the bifurcation point there exist a two-dimensional center manifold to which the dynamics of (A2) will contract. Due to the $Z(2)\times Z(2)$ symmetry, the vector field on the center manifold has the form of (7) with X,Y being coordinates in the null space of the linearization of (A2) for $R=R_k$, $l=l_k$. To compute the coefficients A,B,C,D and α,β one first performs a linear transformation such that the linear part of (A2) becomes diagonal and contains two zeros if $R=R_k$ and $l=l_k$. Schematically the resulting system can be written in the form

$$\dot{X}=\alpha X+N_X\ ,$$
$$\dot{Y}=\beta Y+N_y\ ,$$
$$\dot{Z}_j=\gamma_jZ_j+N_j\quad(1\le j\le 12)\ , \tag{A4}$$

where α, β, and γ_j depend on (R,l) and the N's denote the nonlinear terms. The coefficients α,β vanish for $R=R_k$, $l=l_k$, whereas $\mathrm{Re}(\gamma_j)<0$, i.e., α and β are the unfolding parameters occurring in (7). It remains to compute the nonlinear coefficients A,B,C,D. This is accomplished by setting $R=R_k$, $l=l_k$ ($\alpha=\beta=0$) in (A4), substituting the ansatz $Z_j=P_jX^2+Q_jXY+S_jY^2$ into the Z_j equations with $\dot{X},\dot{Y}$ replaced by N_x,N_y, and then truncating the resulting equations at quadratic order. When comparing the quadratic terms in these equations one obtains a linear algebraic system of equations for the coefficients P_j,Q_j,S_j which can be solved in virtue of $\mathrm{Re}(\gamma_j)<0$. In this way the center manifold has been determined up to second order. If now the $Z_j(X,Y)$ are inserted into the (X,Y) equations of (A4) with terms of higher order than three neglected, ones finds the cubic coefficients A,B,C,D. The details of the computation have been pursued with the aid of the computer algebra system SMP. Sample calculations for the case of ordinary convection (here a nine-mode system is sufficient) can be found in Ref. 1.

APPENDIX B

Setting $l_k\equiv 1$ and defining

$$a^2=a_k^2=k^2+l^2,\ b^2=a_{k+1}^2=(k+1)^2+l^2,\ c^2=1+4l^2,\ d^2=(2k+1)^2+4l^2,\ p=a^6-k^2c^6,\ q=(2k+1)^2a^6-k^2d^6\ ,$$

the analytic expressions for B_{-1}, C_{-1}, etc. are given by

$$B_{-1}=\frac{\pi^2k^2(2k+1)}{16a^2}[-c^2(2k+1)^2(2k+k^2-3l^2)/p+d^2(2k+3k^2+3l^2)/q]\ ,$$

$$C_{-1}=\frac{\pi^2k^2(2k+1)}{16a^2}[c^2(2k+1)^2(-1+k^2-3l^2)/p-d^2(1+4k+3k^2+3l^2)/q]\ ,$$

$$B_0=\frac{a^2\pi^2(2k+1)}{16b^2}\{[a^2(k+1)(2k+3k^2+3l^2)-b^2k(-1+3k^2+3l^2)$$
$$+d^2k(k+1)]/q-(2k+1)[a^2(k+1)(2k+k^2-3l^2)$$
$$+b^2k(1+4k+k^2-3l^2)+c^2k(k+1)(2k+1)]/p\}\ ,$$

$$C_0=\frac{a^2\pi^2(2k+1)}{16b^2}\{-[a^2(k+1)(2+6k+3k^2+3l^2)-b^2k(1+4k+3k^2+3l^2)$$
$$+d^2k(k+1)]/q-(2k+1)[a^2(k+1)(2+2k-k^2+3l^2)$$
$$-b^2k(-1+k^2-3l^2)-c^2k(k+1)(2k+1)]/p\}\ ,$$

$$B_{11}=W_1-W_2+B_{15},\quad B_{12}=W_2-W_1,\quad B_{13}=-2B_{15},\quad B_{14}=W_1+W_2+2B_{15}\ ,$$

$$B_{15}=\{a^6[a^2(k+1)-b^2k][b^2(2k+1)+d^2(k+1)](2k+1)\pi^2\}/(16b^4d^2kq)$$
$$-\{a^6[a^2(k+1)+b^2k][c^2(k+1)+b^2](2k+1)^2\pi^2\}/(16b^4c^2kp)\ ,$$

$$C_{11}=W_1-W_3+C_{15},\quad C_{12}=W_3-W_1,\quad C_{13}=-2C_{15},\quad C_{14}=W_1+W_3+2C_{15}\ ,$$

$$C_{15}=-\{b^2[a^2(k+1)+b^2k](-c^2k+a^2)(2k+1)^2\pi^2\}/[16c^2(k+1)p]$$
$$-\{b^2[a^2(k+1)-b^2k][a^2(2k+1)+d^2k](2k+1)\pi^2\}/[16d^2(k+1)q]\ ,$$

where

$$W_1=[a^2(k+1)^2\pi^2]/(8b^2l^2)\ ,$$

$$W_2=\{[a^2(k+1)-b^2k]\pi^2\}/(16b^2d^2k)-\{[a^2(k+1)+b^2k](2k+1)^2\pi^2\}/(16b^2c^2k)\ ,$$

$$W_3=-\{b^2[a^2(k+1)-b^2k]\pi^2\}/[16a^4d^2(k+1)]-\{b^2[a^2(k+1)+b^2k](2k+1)^2\pi^2\}/[16a^4c^2(k+1)]\ .$$

Numerical values of these coefficients and of l_k and R_{0k} are summarized in Table II for $1\le k\le 10$.

[1]E. Knobloch and J. Guckenheimer, Phys. Rev. A **27**, 408 (1983).

[2]F. Busse and A. C. Or, Z. Angew. Math. Phys. **37**, 608 (1986).

[3]D. Armbruster, Physica **27D**, 433 (1987).

[4]M. Golubitsky and D. Schaeffer, *Singularities and Groups in Bifurcation Theory* (Springer, New York, 1984), Vol. I.

[5]J. K. Platten and G. Chavepeyer, Adv. Chem. Phys. **32**, 581 (1977).

[6]E. Knobloch and M. R. E. Proctor, J. Fluid Mech. **108**, 291 (1981).

[7]J. Guckenheimer and P. Holmes, *Nonlinear Oscillations, Dynamical Systems and Bifurcation of Vector Fields* (Springer, New York, 1983).

[8]M. Neveling, D. Lang, P. Haug, W. Güttinger, and G. Dangelmayr, in *The Physics of Structure Formation,* edited by W. Güttinger and G. Dangelmayr (Springer, New York, 1987).

[9]J. F. Magnan and E. L. Reiss, Phys. Rev. A **36**, 5422 (1987).

[10]D. Armbruster and M. Neveling, J. Non.-Equilib. Thermodyn. **12**, 313 (1987).